

# Melting artificial spin ice

Vassilios Kapaklis,<sup>1</sup> Unnar B. Arnalds,<sup>1</sup> Adam Harman-Clarke,<sup>1,2,3</sup> Evangelos Th. Papaioannou,<sup>1</sup> Masoud Karimipour,<sup>1</sup> Panagiotis Korelis,<sup>1</sup> Andrea Taroni,<sup>1</sup> Peter C. W. Holdsworth,<sup>3</sup> Steven T. Bramwell,<sup>2</sup> and Björgvin Hjörvarsson<sup>1</sup>

<sup>1</sup>*Department of Physics and Astronomy, Uppsala University, Box 516, SE-75120, Uppsala, Sweden*

<sup>2</sup>*London Centre for Nanotechnology, University College London, 17-19 Gordon Street, London WC1H 0AH, UK*

<sup>3</sup>*Université de Lyon, Laboratoire de Physique, École Normale Supérieure de Lyon, 46 Allée d'Italie, 69364 Lyon Cedex 07, France*

Artificial spin ice arrays of micromagnetic islands are a means of engineering additional energy scales and frustration into magnetic materials. Despite much progress in elucidating the properties of such arrays, the ‘spins’ in the systems studied so far have no thermal dynamics as the kinetic constraints are too high. Here we address this problem by using a material with an ordering temperature near room temperature. By measuring the temperature dependent magnetization in different principal directions, and comparing with simulations of idealized statistical mechanical models, we confirm a dynamical ‘pre-melting’ of the artificial spin ice structure at a temperature well below the intrinsic ordering temperature of the island material. We thus create a spin ice array that has real thermal dynamics of the artificial spins over an extended temperature range.

PACS numbers: 75.10.Hk, 75.78.-n

Keywords: Artificial spin ice, Ising model, magnetization dynamics

Geometric frustration is observed in many physical systems. The textbook example is the frustration of proton interactions in water ice, giving rise to proton disorder, as revealed in the pioneering experimental work of Giauque [1] and the theoretical interpretation of Pauling [2]. Frustration in antiferromagnets analogous to the ice model was predicted theoretically by Anderson in 1956 [3]. Only much later was ice-type disorder observed in real magnets, and most surprisingly, this was in ferromagnetic materials, that were thus named ‘spin ice’ [4–6]. The spin ice phenomenon relies on dipole-dipole interactions so the concept was generalized to arrays of magnetic islands with a spin ice type geometry, the ‘artificial’ spin ices [7–13]. Beyond the ice-type systems, the property of frustration is responsible for the occurrence of thermodynamically metastable phases in a variety of systems, including structural (amorphous materials) [14], magnetic (spin glasses) [15] and polymeric systems [16]. In general, the absence of unique ground states [8] and the presence of kinetic constraints [17] makes the study of excitations extremely important. These in combination with the degree of frustration are driving forces for disorder in such systems [18].

The main aim of the present work is to realize a thermodynamic melting transition in an artificial spin ice array. Our work thus represents a significant departure from previous work on artificial spin ice, which have been based on purely mechanical systems, in which the dynamics of the island magnetic moments have been induced by changes in an applied magnetic field, rather than by thermal fluctuations [9, 10]. The use of field-cycling protocols has enabled the realization of quasi-degenerate spin states reminiscent of real spin ice [7, 11], as well as ordered states that are in mechanical equilibrium [12, 13].

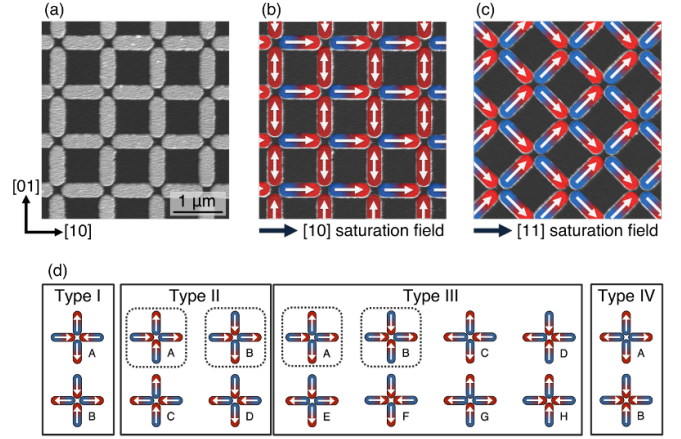


FIG. 1. (a) Atomic Force Microscopy (AFM) image of the artificial square spin ice array. The major symmetry axes are indicated in the lower left corner. (b) Remanent magnetic configuration of the spin ice array after applying a saturation field parallel to the [10] direction and (c) parallel to the [11] direction. (d) The 16 possible remanent magnetic configurations for the artificial square spin ice vertices. After applying a saturation field along the [10] direction there is a fourfold degeneracy of the possible remanent vertex configurations. In comparison, after removing the [11] field, there is only one possible remanent vertex configuration.

While the control and imaging of such systems is impressive, the absence of thermal dynamics means that thermally driven melting, along with other spontaneous dynamical and thermodynamic properties, is not accessible.

To observe the thermally driven melting of an artificial spin ice array experimentally we replace permalloy,

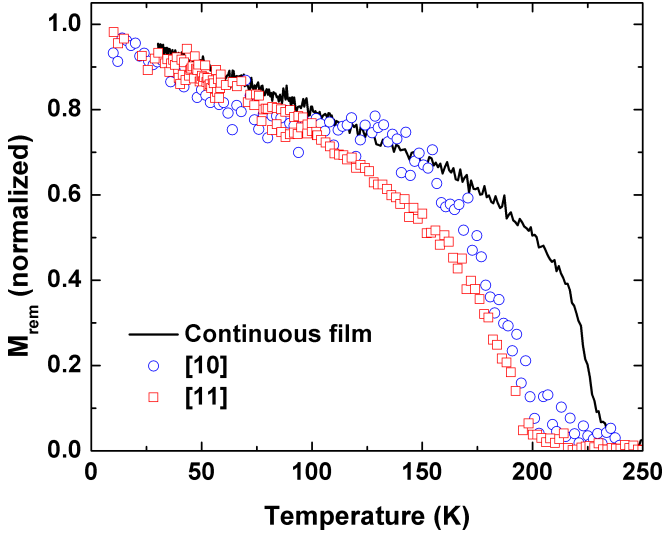


FIG. 2. Normalized remanent magnetization versus temperature curves after a magnetic field has been applied parallel to the [10] and [11] directions with the remanent magnetization of the continuous film used for patterning the arrays. The collapse of the array magnetization at a temperature well below the Curie temperature of the material ( $T_C = 230$  K) is consistent with the appearance of thermally induced dynamics of the macro-spins that comprise the array.

the material that has so far been used most extensively [7, 10, 12], and has a Curie temperature above  $\sim 900$  K, with a film composed of  $\delta$ -doped Pd(Fe). The Curie temperature of the latter can be tuned by variation of the iron (Fe) layer thickness in the palladium (Pd) [19, 20]. For this study we use an Fe layer thickness of 1.2 monolayers (ML) embedded between 10 ML thick Pd layers, giving a Curie temperature of  $T_C = 230$  K. The film was patterned by electron beam lithography and Ar ion milling into an artificial square spin ice array, of  $750 \times 250$  nm<sup>2</sup> islands with a period of 1000 nm, extending over a  $1.5 \times 1.5$  mm<sup>2</sup> area (Fig. 1). The total magnetic moment for each island was determined to be  $M_0 = 1.1 \times 10^{-16}$  Am<sup>2</sup> by superconducting quantum interference device (SQUID) magnetometry measurements performed at 5 K, for a continuous film.

Magnetic hysteresis loops were recorded by means of the magneto-optical Kerr effect (MOKE) technique at temperatures from 5 K to 300 K [20], for an applied field parallel to the [10] and [11] direction of the patterned array (Fig. 1). Figure 2 compares the normalized remanent magnetization,  $M_{\text{rem}}$ , for the magnetic island array with its continuous film counterpart. The remanent magnetizations follow a similar trend up to 100 K, but at higher temperatures the magnetic island array crosses over to a regime in which the magnetization is strongly reduced, approaching zero at around 200 K, while that of the continuous film falls to zero at  $T_C = 230$  K. We argue below,

that this significant difference in behaviour is due to the ‘pre-melting’ of the island array, whose elements retain a finite moment up to the continuous film ordering temperature,  $T_C$ .

In order to discuss the disordering of the magnetic island array, we distinguish between the microscopic magnetic moments within the islands (micro-spins,  $\vec{\sigma}$ ), taken to be of unit length, and the island macro-spins, composed of all  $n$  moments within an island ( $\vec{S} = \sum_{i=1}^n \vec{\sigma}_i / |\sum_{i=1}^n \vec{\sigma}_i|$ ), also of unit length. The coupling between the micro-spins is due to the exchange interaction, with a coupling constant  $J$  related to the  $T_C$  of the magnetic material, while the coupling between the islands is magnetostatic. These interactions are long ranged but the characteristic energy scale can be defined through the interaction between macro-spins,  $\vec{S}$ , on neighboring islands. It turns out that the most relevant interaction is between the next-nearest neighbours, coupling spins along rows or columns of the array. We define this coupling as  $K = K_0 m^2$ , where  $K_0$  is of order  $n^2$  and  $m^2 = \left\langle \left( \frac{1}{n} \sum_{i=1}^n \vec{\sigma}_i \right)^2 \right\rangle$ .

Introducing the thermally averaged quantity  $m^2$  implies that thermal fluctuations of the macro and micro degrees of freedom are decoupled, allowing the two sets to order independently. This assumption could break down for smaller units, in which case the two ordering processes could be renormalized into a single transition, but it should be valid for the islands studied here, consisting of  $\sim 10^7$  micro-spins. Ordering of the macro-spins due to magnetostatic interactions should therefore occur at a temperature  $T_M \leq T_C$ , as even in the limit  $K_0 \gg J$ , the term  $m^2$  ensures that  $K < J$  at  $T_C$ . Thus we predict disordering of the macro-spins at  $T_M$  and a range of temperatures  $T_M < T < T_C$ , in which the islands are decoupled.

The macro-spin  $\vec{S}$  is confined to lie along the long axis of the island through the magnetic shape anisotropy  $K_S$ , which minimizes the collective dipolar energy of an island for the moment in one of the two configurations with Ising symmetry. The energy barrier for reversing the direction of  $\vec{S}$  can be approximated by  $E_r(T) = K_S V$ , with  $K_S(T) = \mu_0 D (M_0 m)^2 / 2$ , and is temperature dependent through  $m^2$ . Here  $\mu_0$  is the permeability of free space,  $D$  is the demagnetization factor of the island, and  $V$  its volume. The macro-spin reversal time scale can be assumed to follow a Néel-Arrhenius law  $\tau = \tau_0 e^{E_r/(k_B T)}$  where  $k_B$  is the Boltzmann constant and for inter-island magnetic fluctuations to occur, this barrier must be thermally accessible. Although an accurate calculation of  $D$  is rather tricky for this material, it can be estimated, assuming the thickness of the active magnetic material to be 1 nm [21]. We choose  $m^2 = (1 - T/T_C)^{2\beta}$ , with  $T_C = 230$  K, and  $\beta = 1/3$ , which matches the temperature vari-

ation of the remanent magnetization of the continuous thin film shown in Fig. 2. This leads to  $E_r = E_0 m^2$ , with  $E_0/k_B \approx 700$  K and  $E_r/(k_B T) = 1$  at 195 K, which ensures accessible thermal fluctuations for macro-spins below  $T_C$ . These estimates could be tested by performing time dependent protocols such as those executed for glassy systems [22], but they suggest that the magnetization data in Fig. 2, include equilibrium thermal fluctuations of Ising-like macro-spins  $\vec{S}$ .

The possible vertex configurations for artificial square spin ice are summarized in Fig. 1(d). Two dimensional square ice does not have the same narrow band of low energy states as three dimensional spin ice, as the long range part of the dipolar interaction is less well screened than in the three dimensional counterpart [23]. As a result, the band of ‘Pauling states’ cannot be considered quasi-degenerate at any level of approximation. The lowest energy configurations are made up of type I vertices, leading to an ordered ground state, with staggered magnetic moments. One might therefore expect to see an ordering phase transition for the macro spins into this state but no such transition is observed. It therefore seems that the type I vertices, which carry no moment, are irrelevant for the low temperature collective phenomena discussed here. The lowest energy states which both satisfy the ice rules and carry a magnetic moment are the subset of type II vertices. Hence the simplest model, that captures the essential physics of this multi-scale problem is a sixteen-vertex model in which the type I states are raised in energy, leaving a four-vertex (type II) manifold of ground states. The validity of this model is tested below through both experiment and numerical simulation.

Within this scenario the application, at low temperature, of a saturation field along the [10] direction would result in a partially lifted degeneracy in favor of the ensemble of states shown in Fig. 1(b), where the macro-spins perpendicular to the applied field, are free to align in the up or down direction. Applying the field along the [11] direction, followed by a return to remanence would lead to the selection of the fully ordered state illustrated in Fig. 1(c). By comparing the ratio of the remanent and saturation magnetization,  $M_{\text{rem}}/M_{\text{sat}}$ , for these two applied field directions (Fig. 3) the island order parameter,  $m^2$ , cancels out, leaving the ordering behaviour of the macro-spins  $\vec{S}$  only. The resulting ratio should therefore be  $1/2$  for the [10] direction and  $1/\sqrt{2}$  for the [11] direction. We measured these ratios for the two applied field directions. In both cases, the measured ratio falls on the prediction to a good approximation up to 125 K, illustrating collective behavior of the macro spins, with a single magnetic domain structure, reminiscent of the four vertex model. Remarkably, the four vertex behaviour, in which vertex defects can be neglected, remains up to temperatures where thermal fluctuations have reduced the squared order parameter of the islands,  $m^2$  to less than half of its zero temperature value. In the case of

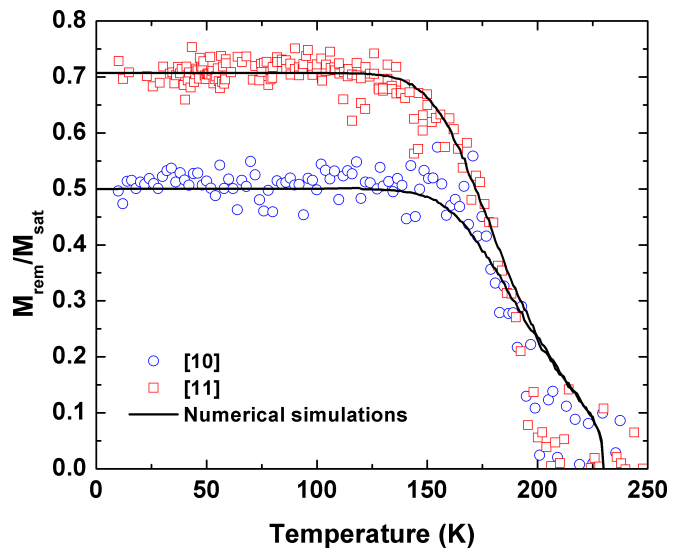


FIG. 3. The ratio of the remanent to saturation magnetization for the array. The ratio is independent of the material magnetization and is a sensitive measure of the order of the macro-spins that constitute the artificial spin ice array. At low temperatures the ratio values of 0.5 and 0.707 for the [10] and [11] direction, respectively, correspond to the array ordered with type II A + B and type III A + B vertices as defined in Fig. 1(d). At higher temperature, the macro-spin order diminishes (‘pre-melts’) at a temperature well below the Curie temperature of the material ( $T_C = 230$  K). The solid black lines are numerical simulations for the 16-vertex model, described in the text, that account for the thermally induced dynamics of the macro-spins. Note that the [11] direction starts to ‘melt’ prior to the [10] direction, suggesting a different accommodation of thermally excited configurations within the artificial square ice array.

the [11] field, the data dips below the  $1/\sqrt{2}$  value at 125 K, while that for the [10] field stays on the line up to a slightly higher temperature, dipping below the expected ratio value at 150 K. The magnetization, for the field applied in both directions, finally collapses as we approach the ordering temperature of the material  $T_C = 230$  K.

To model the experimental data, we consider a sixteen-vertex ice model, of  $N$  Ising spins  $\vec{S}$ , arranged on a square lattice. We raise the energy of type I vertices above those of type II and for simplicity set them equal in energy to the type IV vertices, giving a single energy scale,  $\epsilon_{III} - \epsilon_{II} = K$ ,  $\epsilon_{IV} - \epsilon_{III} = K$ . This model is equivalent to a grill of interpenetrating Ising spin chains coupled uniquely through the first neighbours along the chains [see figure 1(d)]. The ground state is thus an  $\Omega = 2^{2L}$  degenerate manifold of type II states with ferromagnetic ordering along chains (rows) of length  $L = \sqrt{N}/2$  but with disorder among the chains. The parameter  $K$  defines the effective coupling of macro-spins within a chain. At finite temperature, the coupling  $K$  is scaled by  $m^2$ , as defined above. We can also apply a magnetic field whose Zeeman energy scales linearly with the island moment,

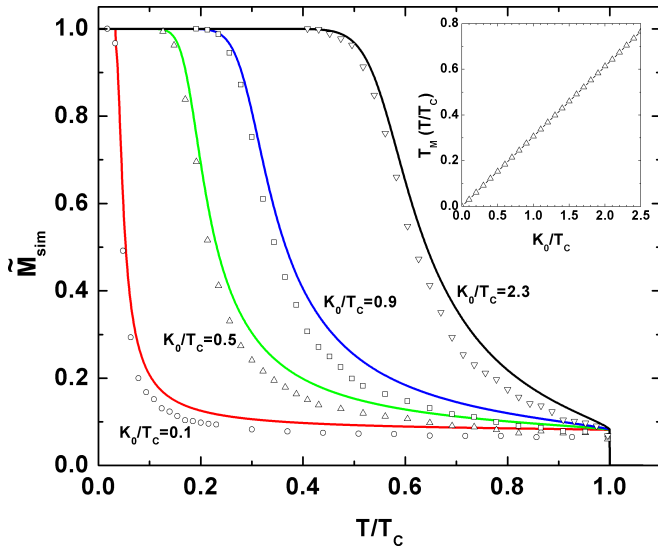


FIG. 4. Illustration of the origin of ‘pre-melting’ in the artificial spin ice array, in terms of the thermal collapse of chain-like correlations between macro-spins. The array is approximated by an assembly of finite length Ising chains that order below a temperature,  $T_M$ , dictated by the interactions between the macro-spins. The points are numerical data from Monte Carlo simulations and the lines the analytical solution for the magnetization of an Ising spin chain of length  $L = 150$ . For temperatures  $T_M < T < T_C$  the macro-spin description is still valid although they are thermally disordered and the magnitude of their collective magnetization tends to that of a paramagnetic chain. The extent of this ‘finite size decoupling’ regime can be varied by changing the strength of the spin coupling in the chain (or on a square ice lattice). Inset: The relation between the spin coupling constant and the ‘pre-melting’ temperature  $T_M$ , extracted from the Monte Carlo simulations. The finite size decoupling regime occurs for any value of the coupling  $K_0$ .

$\sqrt{m^2}$ .

We performed Monte Carlo simulations on a system with  $N = 45000$  macro spins. As expected, there is no phase transition to an ordered state at finite temperature and in zero field the system remains disordered to  $T = 0$ . However the model does have remarkable finite size effects related to the zero temperature critical point of the one dimensional Ising model[24, 25]. This is illustrated in Fig. 4 which shows the temperature evolution of the magnetic moment for macro spins on a single row (or column) of spins,  $\tilde{M}_{\text{sim}} = |\frac{1}{L} \sum_{i=1}^L \tilde{\mathcal{S}}_i|$  for different values of  $K_0/T_C$ . In each case the data are compared with the exact expression for  $\tilde{M}_{\text{sim}}$  for a one dimensional Ising model of  $L$  macro-spins[25], with coupling constant  $K = K_0 m^2$ . The simulation data is indeed reproduced to an excellent approximation by the exact one dimensional result for low values of  $K_0/T_C$ , clearly showing one-dimensional ordering phenomena, even though excitations of the 4-vertex states do communicate between

chains. The chain moment approaches saturation below a crossover temperature, which we can interpret as  $T_M$  when modeling the nano-array. It scales to zero only logarithmically with system size, so that for any reasonable system realisable in the laboratory there is a finite region of temperature for which each chain of the vertex model is ordered.

This finite size chain ordering is at the origin of the observed ‘pre-melting’ as it ensures that the field hysteresis protocol, leading to  $M_{\text{rem}}$ , will order the chains giving a non-zero total moment for the vertex model below this crossover temperature scale. For a field along the [10] direction, the chains parallel to the field will be ordered but those perpendicular will be free, while for the field along [11] all chains should be ordered, as in the experiment. This field induced ordering is confirmed in Fig. 3, where we compare calculated and experimental remanent to saturation magnetization ratio values. The numerical data was taken from simulations using two fitted parameters:  $K_0 \approx 530$  K, corresponding to  $K_0/T_C = 2.3$  (see Fig. 4), and a remanent applied field  $B_0 = 1.8 \times 10^{-5}$  T. The simulation and experimental data are in good agreement up to around 200 K, above which the experimental data falls more rapidly towards zero, which could be due to the development of magnetic fluctuations perpendicular to the Ising spin axis and are not taken into account numerically.

The best fit value of  $K_0$  compares favorably with calculated values: the direct interaction of the island magnetic poles (treated as point charges) yields  $K_0 \approx 530$  K. In addition, this value of  $K_0$  yields a crossover temperature,  $T_M \sim 160$  K which is compatible with the experimental data. The remanent field  $B_0$ , which is required to fit the data, is of a similar magnitude to the earth’s magnetic field and other stray fields that one might expect in a laboratory. Thus, the size of the macro spins means they are extremely sensitive to stray magnetic fields and the non-zero value for  $B_0$  could reflect this. The general agreement between experiment and simulation and the closeness of the fitted parameters to expected values therefore suggests that the sixteen vertex model proposed here, with true thermal dynamics, is indeed an accurate description of the experimental data. The success of the model with type II ground state manifold implies the practical irrelevance of the expected type I ordered ground state. This may be a simple consequence of the fact that for a macro-spin whose total moment exceeds  $10^7$  Bohr magnetons, even a remanent field as small as the earth’s field will push the energy of the type I vertices above the type II states aligned with the field, stabilizing the latter at all times. However, other possible explanations include multipolar interactions, which are known to destabilize type I states in arrays of compass needles [26, 27], and other deviations from ideality such as departures from perfect Ising symmetry of the macrospins. It is also possible that the type I ground state is disfavoured



for purely dynamical reasons [28], or by a mixture of all of the above factors. Further work is needed to clarify this point.

In both experiment and simulation, the crossover from the ordered spin ice regime to the ‘pre-melting’ regime begins at a lower temperature for the [11] field direction than for the [10] direction. ‘Pre-melting’ begins as vertex excitations breaking the ice rules occur, breaking up the correlated chains of macro-spins. In such an excitation, a vertex of type II becomes one of type III through the flipping of the direction of a macro-spin. In the case of remanent magnetization along the [10] direction, there are vertex excitations that preserve the magnetic moment, for example type II  $A + B \rightarrow$  type III  $A + B$ , as illustrated in Fig. 1(d). However, for  $M_{\text{rem}}$  along [11] all excitations are moment reducing. This suggests that the magnetization ratio will remain near the upper bound in the first stages of ‘pre-melting’ for ordering along [10] while the ratio will be reduced from this bound as soon as defects appear, for ordering along [11]. These defects carry accumulations of effective magnetic charge and in the case of three dimensional spin ice, have been successfully described using the language of emergent magnetic monopoles [29–31]. In this case, the term ‘monopole’ should be used with great caution, as long ranged interactions are less well screened for four-fold symmetry in a plane, than in spin ice. However, it will nevertheless be interesting to study the dynamic and static properties of these excitations in future work.

In conclusion, we have argued that through careful control of the relative strength of the interactions in an artificial square spin ice we can access a ‘finite size decoupling’ regime in which true thermodynamic properties are present. Having applied this to an experimental array based on  $\delta$ -doped Pd(Fe), we have demonstrated, using a thermodynamic measurement, the existence of the ‘pre-melting’ of the array indicating just such a ‘finite size decoupling’ regime. This is clearly a general approach which will allow the design of spin ice arrays with a wide range of dynamic properties.

The authors acknowledge the support of the Swedish Research Council (VR), the Knut and Alice Wallenberg Foundation (KAW), the Swedish Foundation for International Cooperation in Research and Higher Education (STINT), the Icelandic Research Fund for Graduate Students and the Institut Universitaire de France (IUF). S.T.B. thanks the UK EPSRC for financial support. The patterning was performed at the Center for Functional Nanomaterials (CFN), Brookhaven National Laboratory, which is supported by the U.S. Department of Energy, Office of Basic Energy Sciences, under Contract No. DE-AC02-98CH10886. V.K., U.B.A. and B.H. thank Aaron Stein for support received during pattern-

ing at CFN. A.H.-C. thanks Simon Banks for valuable discussions.

- 
- [1] W. F. Giauque and J. W. Stout, *Journal of the American Chemical Society*, **58**, 1144 (1936).
  - [2] L. Pauling, *Journal of the American Chemical Society*, **57**, 2680 (1935).
  - [3] P. W. Anderson, *Phys. Rev.*, **102**, 1008 (1956).
  - [4] M. J. Harris, S. T. Bramwell, D. F. McMorrow, T. Zeiske, and K. W. Godfrey, *Phys. Rev. Lett.*, **79**, 2554 (1997).
  - [5] A. P. Ramirez et al., *Nature*, **399**, 333 (1999).
  - [6] S. T. Bramwell and M. J. P. Gingras, *Science*, **294**, 1495 (2001).
  - [7] R. F. Wang et al., *Nature*, **439**, 303 (2006).
  - [8] P. E. Lammert et al., *Nature Physics*, **6**, 786 (2010).
  - [9] S. Ladak et al., *Nature Physics*, **6**, 359 (2010).
  - [10] E. Mengotti et al., *Nature Physics*, **7**, 68 (2010).
  - [11] J. Cumings, *Nature Physics*, **7**, 7 (2011).
  - [12] J. P. Morgan et al., *Nature Physics*, **7**, 75 (2011).
  - [13] A. Schumann et al., *Appl. Phys. Lett.*, **97**, 022509 (2010).
  - [14] O. N. Senkov and D. B. Miracle, *Materials Research Bulletin*, **36**, 2183 (2001).
  - [15] S. Kirkpatrick, *Phys. Rev. B*, **16**, 4630 (1977).
  - [16] G. I. Menon and R. Pandit, *Phys. Rev. Lett.*, **75**, 4638 (1995).
  - [17] F. Ritort and P. Solich, *Adv. Phys.*, **52**, 219 (2003).
  - [18] H. J. Fecht, *Nature*, **356**, 133 (1992).
  - [19] M. Pärnaste et al., *Journal of Physics: Condensed Matter*, **19**, 246213 (2007).
  - [20] E. Th. Papaioannou et al., *Journal of Physics: Condensed Matter*, **22**, 236004 (2010).
  - [21] J. A. Osborn, *Phys. Rev.*, **67**, 351 (1945).
  - [22] J. P. Bouchaud et al., in *Spin glasses and random fields*, Vol. 12, edited by A. P. Young (World Scientific, Singapore, 1998).
  - [23] S. V. Isakov, R. Moessner, and S. L. Sondhi, *Phys. Rev. Lett.*, **95**, 217201 (2005).
  - [24] E. Ising, *Z. Phys.*, **31**, 253 (1925).
  - [25] The finite size Ising chain is often discussed in passing as a prelude to results in the thermodynamic limit. Two recent papers that focus on the model in its own right are Y. Li and B.-G. Liu, *Phys. Rev. B* **73**, 174418 (2006) and V. I. Belokon’ et al., *Bulletin of the Russian Academy of Sciences: Physics* **74**, 1413 (2010). The exact analytical expression is:  $\langle \tilde{M}_{\text{sim}}(T) \rangle = \left( \frac{1}{L} \exp \left( \frac{2K}{T} \right) \frac{1 - \tanh(\frac{K}{T})^L}{1 + \tanh(\frac{K}{T})^L} \right)^{\frac{1}{2}}$ .
  - [26] E. Olive and P. Molho, *Phys. Rev. B*, **58**, 9238 (1998).
  - [27] E. Y. Vedmedenko, N. Mikuszeit, H. P. Oepen, and R. Wiesendanger, *Phys. Rev. Lett.*, **95**, 207202 (2005).
  - [28] A. Remhof et al., *Phys. Rev. B*, **77**, 134409 (2008).
  - [29] C. Castelnovo, R. Moessner, and S. L. Sondhi, *Nature*, **451**, 42 (2008).
  - [30] L. D. C. Jaubert and P. C. W. Holdsworth, *Nature Physics*, **5**, 258 (2009).
  - [31] S. R. Giblin et al., *Nature Physics*, **7**, 252 (2010).